Polymer Chemistry

Accepted Manuscript

This is an *Accepted Manuscript*, which has been through the Royal Society of Chemistry peer review process and has been accepted for publication.

Accepted Manuscripts are published online shortly after acceptance, before technical editing, formatting and proof reading. Using this free service, authors can make their results available to the community, in citable form, before we publish the edited article. We will replace this *Accepted Manuscript* with the edited and formatted *Advance Article* as soon as it is available.

You can find more information about *Accepted Manuscripts* in the Information for Authors.

Please note that technical editing may introduce minor changes to the text and/or graphics, which may alter content. The journal's standard Terms & Conditions and the Ethical guidelines still apply. In no event shall the Royal Society of Chemistry be held responsible for any errors or omissions in this *Accepted Manuscript* or any consequences arising from the use of any information it contains.

ROYAL SOCIETY OF CHEMISTRY

www.rsc.org/polymers

Journal Name

ARTICLE

Highly Crystalline, Low Band-gap Semiconducting Polymers Based on Phenanthrodithiophene-benzothiadiazole for Solar Cells and Transistors

Received 00th January 20xx,
Accepted 00th January 20xx

DOI: 10.1039/x0xx00000x

www.rsc.org/

Hiroki Mori,[a] Hikaru Nonobe[a] and Yasushi Nishihara*[a]

New PDT-based polymers combine with two types of benzothiadiazole (BT) derivatives to improve their crystallinity and solar cell performance. These polymers present several advantages, including strong intermolecular interactions, deep HOMO energy levels, and a dense packing structure with the short π-π stacking distance of 3.5~3.6 Å. Combinations of PDT and BT units in polymers formed highly crystalline thin films with long-range order, even in films blended with a fullerene derivative. This suggests that the introduction of optimal acceptor units may increase the regularity of the polymers, leading to effective π-π overlaps between polymer backbones. However, although the present polymers also formed an appropriate phase separation structure in blended films, in fabricated solar cell devices they yielded low power conversion efficiencies (PCEs) not exceeding 3.8%. GI-WAXS analysis revealed that both polymers were present in a predominantly edge-on orientation. This unsuitable orientation for PSCs prevented efficient carrier transport and reduced charge collection efficiency, resulting in low J_{sc}, and thus low PCE. On the other hand, these polymers also formed highly oriented edge-on structures on n^+-Si/SiO_2 substrates, which is suitable for high-performance field-effect transistors (FETs), and a fabricated FET device showed hole mobility as high as 0.18 $cm^2 V^{-1} s^{-1}$.

Dedicated to Professor Kohtaro Osakada on occasion of his 60th birthday.

Introduction

Solar cells have gained serious attention because they are the most useful, environmentally clean, and renewable energy source that can replace conventional fossil fuels. In a field with several contenders, semiconducting polymer-based solar cells (PSCs) are among the more promising candidates for next-generation solar-energy conversion because of their potential features, including light weight, flexibility and stretchability, large area, low cost, and low-energy manufacturing processes.[1-6] In the past decade, various types of donor-acceptor (D-A) semiconducting polymers have been developed with power conversion efficiency (PCE) exceeding 10% in single-junction solar cells.[7-10] However, examples of such high-performance D-A polymers are somewhat limited, so further development of new D-A polymers is a high priority.

When designing high-performance D-A polymers, the optimal combination of electron-donor and electron-acceptor units is quite important. Typically, HOMO and LUMO energy levels of D-A polymers are strongly influenced by the HOMO of the donor and the LUMO of the acceptor.[11-15] Thus one can tune the energy levels to obtain polymers with the desired strong and wide absorption range and deep HOMO energy level. Other key factors for a high-performance PSC are crystallinity and thin-film structure. Most high-performance polymers form highly crystalline solids with a strongly long-range-ordered structure that can transport charge carriers effectively.[7,9,16-21] Moreover, such highly crystalline polymers tend to provide an optimal phase separation structure in bulk-heterojunction films, which can enhance both exciton dissociation efficiency and charge carrier mobility.[22,23] Highly crystalline polymers must have a strong self-assembling tendency in the solid state.

With these factors in mind, we have focused on the development of highly extended π-electron systems and their incorporation in a polymer backbone to enhance intermolecular interactions. Recently, we have developed phenanthro[1,2-*b*:8,7-*b*']dithiophene (PDT)[24-27] as a new extended π-electron building unit, and PDT-based D-A polymers.[28-30] These PDT-based polymers have strong intermolecular interactions, deep HOMO energy levels, and a dense π-stacking structure with a short π-π stacking distance of 3.5~3.6 Å, all features that are useful in PSCs. In fact, PDT-

[a] Division of Earth, Life, and Molecular Sciences, Graduate School of Natural Science and Technology, Okayama University, 3-1-1 Tsushimanaka, Kita-ku, Okayama 700-8530, Japan. E-mail: ynishiha@okayama-u.ac.jp.

Electronic Supplementary Information (ESI) available: [Full characterizations of all new compounds, as well as details of physicochemical properties, surface morphologies and device characteristics]. See DOI: 10.1039/x0xx00000x

isoindigo copolymers with optimal side chains showed good solar-cell performance, with PCE over 5%[29] and good carrier transporting ability, with hole mobility of up to 0.16 $cm^2 V^{-1} s^{-1}$.[30] However, most PDT-based polymer films on an ITO/ZnO substrate have low crystallinity, in spite of an optimal phase separation structure, which may limit their device performance. In general, typical dyes/pigments such as diketopyrrolopyrrole or isoindigo have a strongly polarized core, which dramatically increases the intermolecular interactions of polymers.[31,32] This requires a number of longer or bulkier alkyl side chains to ensure their solubility. However, the side chains often interfere with effective π-π overlap, leading to low crystallinity.

In this study, we designed new PDT-based polymers (Scheme 1, **P-PDT-(DF)BT-DT**) combined with benzothiadiazole (BT) derivatives to improve crystallinity and device performance. BT is one of the most widely used acceptor units for high-performance organic electronics, with strong electron affinity and a deep HOMO energy level.[7,12,15,19,21,33-47] In combination with PDT as a weak electron-donor unit, HOMO coefficients delocalize over the end of a PDT moiety, as is evident from DFT calculations on a model compound (Figure 2). These target polymers can retain a deep HOMO energy, and their HOMO orbital can enhance their intermolecular interactions. In addition, incorporation of a non-polar BT core into a PDT-based polymer backbone can improve solubility without any bulky solubilizing groups, potentially yielding high crystallinity. Moreover, adding a BT core to a PDT-based polymer backbone with C_{2v} symmetry can increase regularity so the alkyl side chains point in the same direction, which can enhance effective π-π overlap to yield highly crystalline films.[48,49] The BT core can easily have two fluorine atoms, yielding further enhancement of intermolecular interactions and deeper HOMO energy levels.[19,21,50-53] Herein, we report the synthesis and characterization of the new PDT-based polymers **P1** and **P2,** containing BT or difluorinated BT (DFBT), and evaluate the relationship between device performance and specific structures and molecular orientations in the solid state.

Experimental

General

All the reactions were carried out under an Ar atmosphere using standard Schlenk techniques. Glassware was dried in an oven (130 °C) and heated under reduced pressure prior to use. Dehydrated solvents were purchased from Kanto Chemicals Co., Ltd. For thin layer chromatography (TLC) analyses throughout this work, Merck pre-coated TLC plates (silica gel_{60} GF_{254}, 0.25 mm) were used. Silica gel column chromatography was carried out using Silica gel 60 N (spherical, neutral, 40-100 μm) from Kanto Chemicals Co., Ltd. The ^1H and $^{13}C\{^1H\}$ NMR spectra were recorded on Varian 400-MR (400 MHz) spectrometer. Elemental analyses were carried out with a Perkin-Elmer 2400 CHN elemental analyser at Okayama University. Polymerization was performed with a Biotage initiator microwave reactor. Molecular weights of polymers were determined by gel-permeation chromatography (GPC) with a Senshu Scientific SSC-7120 using polystyrene standard and *o*-dichlorobenzene (DCB) as the eluent at 140 °C.

4,7-Dibromobenzo[*c*][1,2,5]thiadiazole[54], 4,7-bis(4-(2-decyltetradecyl)thiophen-2-yl)benzo[*c*][1,2,5]thiadiazole[55], 4,7-bis(5-bromo-4-(2-decyltetradecyl)thiophen-2-yl)benzo[*c*]-[1,2,5]thiadiazole (**1**)[55], 5,6-difluoro-4,7-dibromobenzo-[c][1,2,5]-thiadiazole[53,56], 5,6-difluoro-4,7-bis(4-(2-decyltetra-decyl)thioph-en-2-yl)benzo[*c*][1,2,5]thiadiazole[57], 5,6-difluoro-4,7-bis(5-bromo-4-(2-decyltetradecyl)thiophen-2-yl)benzo[*c*][1,2,5]thiadiazole (**2**)[57], and 2,9-bis(trimethylstannyl)phenanthro[1,2-*b*:8,7-*b*']dithiophene (**3**)[28] were synthesized by previously reported procedures.

Poly[phenanthro[1,2-*b*:8,7-*b*']dithiophen-2,9-diyl-*alt*-5,5-(4',7'-bis[4-(2-decyltetradecyl)-thienyl]-benzo[*c*][1,2,5]thia-diazole)] (P1). **3** (61.6 mg, 0.10 mmol), **1** (113.1 mg, 0.10 mmol), $Pd(PPh_3)_4$ (2.3 mg, 2.0 μmol), and toluene (5 mL) were added in a reaction vessel. The vessel was sealed and refilled with argon, and was put into a microwave reactor and heated to 180 °C for 40 min. After cooling to room temperature, the reaction solution was poured into 100 mL of methanol containing 5 mL of hydrochloric acid and stirred for 12 h. The precipitate was then subjected to sequential Soxhlet extraction with methanol, hexane, and chloroform to remove low molecular weight fraction. The residue was extracted with chlorobenzene and precipitated in 100 mL of methanol. The precipitate was collected by filtration and dried in vacuo to afford the polymer sample (111.1 mg, 88%) as a bright purple solid. GPC (DCB, 140 °C): M_n = 37.9 kDa, M_w = 64.3, PDI = 1.70). Anal. Calcd for $C_{80}H_{112}N_2S_5$: C, 76.13; H, 8.94; N, 2.22. Found: C, 75.96; H, 8.33; N, 2.21.

Poly[phenanthro[1,2-*b*:8,7-*b*']dithiophen-2,9-diyl-*alt*-5,5-(5',6'-difluoro-4',7'-bis[4-(2-decyltetradecyl)-thienyl]-benzo[*c*][1,2,5]-thiadiazole)] (P2). **3** (30.9 mg, 0.05 mmol), **2** (58.4 mg, 0.05 mmol), $PdCl_2(PPh_3)_2$ (0.7 mg, 1.0 μmol), and toluene (2.5 mL) were added in a reaction vessel. The vessel was sealed and refilled with argon, and was put into a microwave reactor and heated to 110 °C for 30 min. After cooling to room temperature, the reaction solution was poured into 100 mL of methanol containing 5 mL of hydrochloric acid and stirred for 12 h. The precipitate was then subjected to sequential Soxhlet extraction with methanol, hexane, and chloroform to remove low molecular weight fraction. The residue was extracted with chlorobenzene and precipitated in 100 mL of methanol. The precipitate was collected by filtration and dried in vacuo to afford the polymer sample (59.5 mg, 90%) as a bright purple solid. ^1H NMR (600 MHz, toluene-d_8, 80 °C): δ 0.8-2.4 (brs, 92H), 2.xx (brs, 2H), 3.14 (brs, 4H), 7.2-8.5 (brs, 10H). GPC (DCB, 140 °C): M_n = 15.9 kDa, M_w = 20.3, PDI = 1.28). Anal. Calcd for $C_{80}H_{110}F_2N_2S_5$: C, 74.02; H, 8.54; N, 2.16. Found: C, 73.06; H, 7.81; N, 2.16.

Instrumentation and Theoretical Calculations

Thermogravimetric analyses (TGA) were carried out using a TG/DTA 6300 (SII Nanotechnology, Inc.) at 10 °C/min under a N_2 atmosphere. Differential scanning calorimetry (DSC) was performed on a Mettler Toledos DSC-1 at 10 °C/min for both heating and cooling steps. UV-vis absorption spectra were measured using a Shimadzu UV-2450 UV-vis spectrometer. Cyclic voltammograms (CVs) were recorded on Electrochemical Analyser CHI-600B in acetonitrile containing tetrabutylammonium hexafluorophosphate (TBAP, 0.1 M) as supporting electrolyte at a scan rate of 100 mV/s. A Pt electrode (surface area: A = 0.071 cm^2, BAS), an Ag/Ag^+ (Ag wire in 0.01 M $AgNO_3$/0.1 M TBAP/CH_3CN), and a Pt wire electrode were used as working, reference, and counter electrodes, respectively. Samples of the polymer films were prepared by drop-casting on a working electrode from their chloroform solutions. All the potentials were calibrated with the standard ferrocene/ferrocenium redox couple (Fc/Fc^+: $E^{1/2}$ = +0.08 V measured under identical conditions). Dynamic force mode atomic force microscopy was carried out using an SPA 400-DFM (SII Nano Technologies). Grazing incidence wide-angle X-ray scattering (GI-WAXS) analyses were carried out at SPring-8 on beamlines BL19B2 and BL46XU. The samples were irradiated at a fixed angle on the order of 0.12° through a Huber diffractometer with an X-ray energy of 12.39 keV (λ = 1 Å), and the GI-WAXS patterns were recorded on a 2D image detector (Pilatus 300K). Films of the polymers with or without $PC_{61}BM$ were fabricated by spin-coating on the ZnO treated ITO substrate and octadecyltriethoxysilane (ODTS) treated n^+-Si/SiO_2 substrate. Geometry optimizations and normal-mode calculations were performed at the B3LYP/6-31G(d) level using the Gaussian 09, Revision A. 02, program package.[58]

Fabrication and Characterization of Solar Cell Devices

The inverted bulk-heterojunction (BHJ) PSCs were fabricated as follows. ZnO precursor solution was prepared by hydrolysis of $Zn(OAc)_2$.[59] The ITO substrates (ITO, Geomatec Co. Ltd., thickness = 150 nm, sheet resistance < 12 Ω sq^{-1}, transmittance (λ = 550 nm) ≧ 85%) were successively washed using ultrasonication in a neutral detergent, deionized water, acetone, and isopropanol for 10 min, respectively. Then ITO substrate was treated with UV-ozone for 20 min. Pre-cleaned ITO substrates was spin-coated with 0.2 M ZnO precursor solution at 4000 rpm for 30 sec, and then immediately baked at 200 °C for 30 min in air. After gradually cooling to room temperature, the substrates were rinsed with acetone and isopropanol. The substrates were dried and immediately transferred into a nitrogen filled glove box. The thin film of active layer was deposited by spin-coating from an anhydrous chlorobenzene (CB) blended solution containing 7.5~10 mg/mL polymer samples with same amount of $PC_{61}BM$ at 400 rpm for 30 sec, and 1000 rpm for 5 sec. After drying the thin films, a MoO3 (6 nm) as an anode interlayer and Ag (50 nm) was deposited under high vacuum (~3×10^{-5} Pa) through the shadow mask. The active area of all devices was 0.16 cm^2.

The characteristics of the solar cell devices were measured through a 4 × 4 mm photo-mask with a Keithley 2401 semiconducting analyser using a Xe lamp (Bunkokeiki OTENTO-SAN III type G2) as the light source under AM 1.5 G simulated solar irradiation at 100 $mWcm^{-2}$ at room temperature in an inert atmosphere. The light intensity was determined by calibrated standard silicon solar cell (Bunkokeiki, BS-520BK). External quantum efficiency (EQE) was measured using a Bunkokeiki SM-250 hyper monolight system

Fabrication and Characterization of Transistor Devices

The typical bottom-gate top-contact OFET devices were fabricated as follows. All the processes, except for substrate cleaning, were performed under an inert condition. Heavily doped *n*-Si wafer with 200 nm-thick thermally grown SiO_2 (C_i = 17.3 nF cm^{-2}) as dielectric layer was used as the substrate. The Si/SiO_2 substrates were carefully cleaned using ultrasonication with deionized water, acetone, and isopropanol, respectively. After drying the substrates, they were irradiated UV-O_3 for 20 min and then treated with octadecyltriethoxysilane (ODTS) to form a self-assembled monolayer (SAM). The active layers were deposited on the treated substrate by spin-coating from *o*-dichlorobenzene (DCB) solution (3 gL^{-1}) at 3000 rpm for 30 sec. After drying or annealing at 250~300 °C for 30 min, gold electrode (80 nm thick) was deposited through a shadow mask on the top of the active layer under reduced pressure (~5×10^{-5} Pa). For typical device, the source-drain channel length (L) and width (W) are 100 μm and ca. 2 mm, respectively.

The current-voltage characteristics of the OFET devices were measured at room temperature in air on a Keithley 6430 sub-femto ampere remote source meter combined with Keithley 2400 measure-source unit. Field-effect mobilities in saturation regime were calculated by following equation,

$$I_D = (WC_i/2L)\,\mu\,(V_G - V_{th})^2$$

where C_i is the capacitance of the SiO_2 insulator, and V_G, V_{th}, and I_D are the gate and threshold voltages, and source-drain current, respectively. Current on/off ratio ($I_{on/off}$) was determined from a minimum I_D at around V_G = 0~10 V and maximum I_D at V_G = −60 V. The parameters of all devices were collected from more than five different devices.

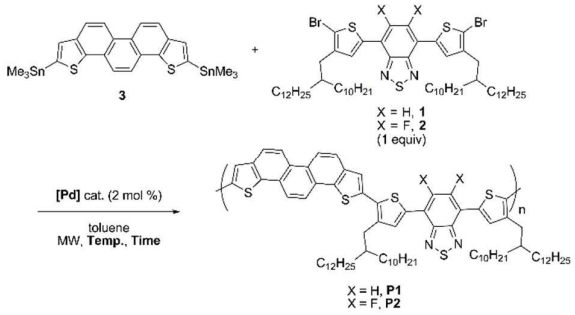

Scheme 1 Synthesis of P-PDT-(DF)BT-DT copolymers

Table 1 Results of polymerization

X	[Pd] cat.	Temp. /°C	Time /min	M_n /kDa[a]	M_n /kDa[a]	PDI[a]
H	$Pd(PPh_3)_4$	180	40	37.9	64.3	1.70
F	$PdCl_2(PPh_3)_2$	110	30	15.9	20.3	1.28

[a]Determined by GPC measurement using polystyrene standard and *o*-dichlorobenzene (DCB) as the eluent at 140 °C.

Results and Discussion

Synthesis and GPC Analysis of the Polymers

Scheme 1 shows the synthesis of the two target copolymers using PDT and BT derivatives. Migita-Kosugi-Stille coupling of **1** and **3** afforded **P1** as a soluble product in hot chlorobenzene. The number-average molecular weight (M_n) and polydispersity index (PDI) of the obtained polymer were 37.9 kDa and 1.70, sufficient for use in organic electronic devices. In contrast, when **P2** was synthesized by copolymerization of **2** with **3** under the same conditions, the obtained polymer was completely insoluble, even in hot chlorobenzene. Then we optimized polymerization conditions to yield soluble **P2**. Copolymerization at low temperature with a different catalyst system yielded soluble **P2** in 90% yield. The molecular weight of the obtained **P2** is 15.9 kDa, approximately half that of **P1**. These results indicate that increased coplanarity of PDT-BT polymers may enhance intermolecular interactions, but significantly decrease solubility.

Physicochemical Properties

TGA and DSC measurements were performed to evaluate thermal stability (Figures S1 and S2). The 5% weight loss temperatures (T_d^5) of the obtained polymers are 317 °C for **P1** and 309 °C for **P2**, respectively. In addition, transition peaks such as glass transition and melting point were not observed up to 250 °C, indicating high thermal stability for both polymers.

Depicted in Figure 1 are UV-vis absorption spectra of the polymers in chlorobenzene and as thin films. Both **P1** and **P2** exhibited a broad absorption range around 700 nm with respective optical energy gaps of 1.63 and 1.65 eV as thin films. Fluorine-substituted polymer **P2** had slightly blue-shifted spectra and a larger energy gap than **P1**, as typically seen in fluorine-containing polymers.[53,60] While the spectrum of **P1** in the solid state is slightly red-shifted as compared to that in solution, three shoulder peaks at 560, 601, and 651 nm disappeared and a significantly blue-shifted spectrum was observed when heated to ca. 80 °C, which reflects the complete disaggregation of the polymer. In contrast, the spectrum of **P2** in solution at room temperature is almost identical to that of its thin film. In addition, two defined peaks derived from vibronic transitions remained present in hot chlorobenzene solution, implying that **P2** forms large aggregates even in that high-temperature solution. This indicates that **P2** has stronger intermolecular interactions than **P1**.

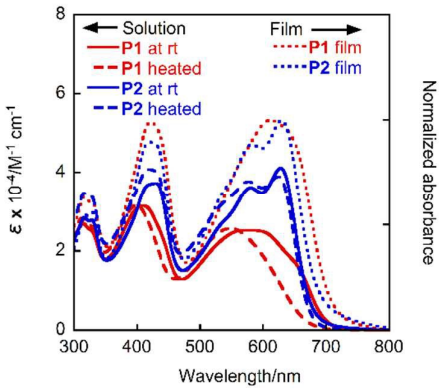

Figure 1 UV-vis absorption spectra of **P1** and **P2** in chlorobenzene solution and in thin film.

Table 2 Physicochemical Properties of **P1** and **P2**

polymer	$\lambda_{max,rt}$ ($\lambda_{max,heated}$)/nm[a]	λ_{max}/nm[b]	E_g^{opt}/eV[c]	E_{HOMO}/eV[d]	E_{LUMO}/eV[e]
P1	561, 601, 651 (549)	612, 647	1.63	−5.28	−3.66
P2	580, 628 (577, 624)	582, 630	1.65	−5.42	−3.70

[a]Absorption maxima in solution at room temperature and ca. 80 °C. [b]Absorption maxima in thin films. [c]Optical energy gaps in thin film estimated from absorption edge (λ_{edge}). [d]Estimated from the oxidation onset vs. Ag/Ag^+ calibrated with Fc/Fc^+; $E_{HOMO} = -4.72 - E^{ox}_{onset}$. [e]Estimated with the following equation; $E_{LUMO} = -4.72 - E^{red}_{onset}$.

To investigate the effect of fluorine atoms on the electronic structure of the polymers, we measured their cyclic voltammograms (CV) in the solid state (Figure S3); extracted parameters are summarized in Table 2. Both **P1** and **P2** showed clear oxidation and weak reduction peaks. The estimated LUMO energy level of **P2** is −3.70 eV, which is slightly lower than that of **P1** (−3.66 eV). This might represent enhancement of its electron affinity due to the introduction of fluorine, but both polymers have sufficiently low LUMO energy levels for charge separation and electron transfer without any energy losses. The HOMO energy level of **P2** (−5.42 eV) was also deeper than that of **P1** (−5.28 eV), owing to the strong electron-withdrawing nature of two fluorine atoms. Therefore, a **P2**-based PSC would be expected to show a higher V_{oc}, because V_{oc} generally depends on the energy difference between the HOMO of the donor polymer and the LUMO of fullerene derivatives.[61]

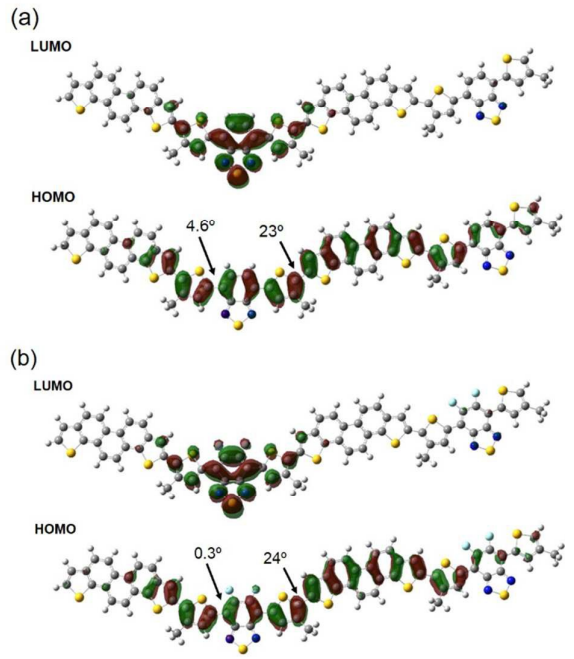

Figure 2 Optimized HOMO and LUMO orbitals of model compound calculated by DFT at B3LYP/6-31G(d); (a) **P1** and (b) **P2**.

The molecular orbital distribution and dihedral angle of the polymers were calculated by density functional theory (DFT) at B3LYP/6-31G(d) using their dimer structure as the model compound (Figure 2). The LUMO orbital of both polymers is well localized on the benzothiadiazole moiety, while the HOMO coefficient of both polymers is delocalized over the polymer backbone. This tendency is typical of D-A polymers with weak donor and strong acceptor moieties.[62] Both HOMO and LUMO coefficients are also delocalized on fluorine atoms, which may stabilize HOMO and LUMO energy levels. In fact, the calculated HOMO and LUMO energy levels of the model compound in **P2** (−5.14 and −2.74 eV) are higher than that of **P1** (−5.02 and −2.67 eV), which is consistent with the results of CV measurement. Because of steric crowding between the sulfur atoms of PDT and the alkyl side chains on the thiophene spacer, the dihedral angle between PDT and thiophene in both polymers is 23~24°. On the other hand, fluorinated polymer **P2** has a smaller dihedral angle (0.3°) between thiophene and benzothiadiazole units than **P1** has (4.6°), owing to the substitution of relatively small fluorine atoms and the influence of an F···S interaction.[50] This higher coplanarity of **P2** can enhance the intermolecular π-orbital overlap adjacent to the polymer backbone. Thus, **P2** should display stronger intermolecular interactions, which is in good agreement with UV-vis absorption measurements.

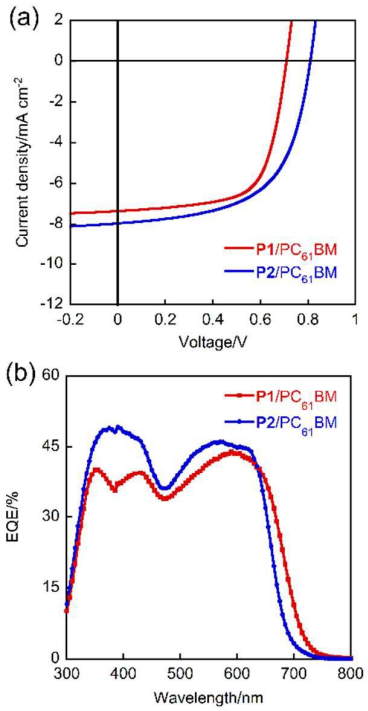

Figure 3 (a) *J-V* curves of **P1** or **P2**-based inverted solar cells and (b) corresponding EQE spectra.

Characteristics of Inverted Bulk-heterojunction Solar Cells

To investigate the solar cell performance of polymer**s**, inverted bulk-heterojunction solar cell devices with the configuration of ITO/ZnO/(**P1** or **P2**:$PC_{61}BM$)/MoO_3 (6 nm)/Ag (50 nm) were fabricated and characterized. Figure 3a shows typical current density-voltage (*J-V*) characteristics under AM 1.5 G simulated solar irradiation of the fabricated solar cells at 1 sun (100 mW cm^{-2}), and their best photovoltaic properties are summarized in Table 3. The **P1**-based inverted cell exhibited a power conversion efficiency (PCE) of 3.48%, with a J_{sc} of 7.35 $mAcm^{-2}$, a V_{oc} of 0.71 V, and an FF of 0.67. On the other hand, the **P2**-based cell showed the slightly higher PCE of 3.79% with a J_{sc} of 7.96 $mAcm^{-2}$, a V_{oc} of 0.81 V, and an FF of 0.59, though the **P2** had a lower molecular weight. In general, solar cell performance depends strongly on the molecular weight of the polymer, and a cell using low molecular-weight polymers often shows poor photovoltaic properties.[41,63-65] As expected from the deep HOMO energy levels estimated by CV measurements, the **P2**-based cell showed a higher V_{oc} than that of the **P1**-based cell. From the EQE spectra in Figure 3b, although the EQE values of both polymer-based cells around 500-700 nm were almost the same (~45%), the EQE in the shorter wavelength region of **P2** was about 10% higher than that of **P1**, resulting in a higher J_{sc}. Although **P2** thin film have weak absorption at around 400 nm relative to the **P1** thin film, the higher EQE of **P2**-based cell at shorter wavelength region may contribute to higher photocurrent conversion from $PC_{61}BM$, likely owing to the difference of their morphologies. These results indicate that the substitution of fluorine atoms for hydrogens can enhance the photovoltaic performance of a PDT-based polymer system. However, the solar cell performance of these PDT-based polymers is still lower than

that of previously reported PDT-IID copolymers.[29] The main reason for their lower performance is the relatively low J_{sc} (~8 mA cm^{-2}) in these polymer-based cells compared with typical high-performance D-A polymers,[11-15] and approximately 50% of incident light did not contribute to the photocurrent conversion, as is evident from their EQE spectra.

Table 3 Photovoltaic Properties of inverted solar cells

polymer	J_{sc}/mA cm^{-2}	V_{oc} /V	FF	PCE$_{max}$ (PCE$_{avg}$)[a]
P1	7.35	0.71	0.67	3.48 (3.26)
P2	7.96	0.81	0.59	3.79 (3.41)

[a]Average values based on 16 devices.

To gain an insight into the effect of the polymers' morphology, we investigated the surface morphology of two polymers in films blended with PC$_{61}$BM by using atomic force microscopy (AFM), as shown in Figure 4. Topological images of both **P1** and **P2** blended films showed a uniform structure with a texture displaying small spherical shapes on the surface. **P2**/PC$_{61}$BM film, with a root-mean-square unevenness of 2.87 nm, is rougher than **P1**/PC$_{61}$BM film (RMS = 0.88 nm), but both films have well-separated structures (domain size: 10~40 nm) with an optimal interpenetrating network. This appropriate micro-phase separation structure is likely to enable efficient charge separation and carrier transport,[22,23,66] which will not limit their PCE.

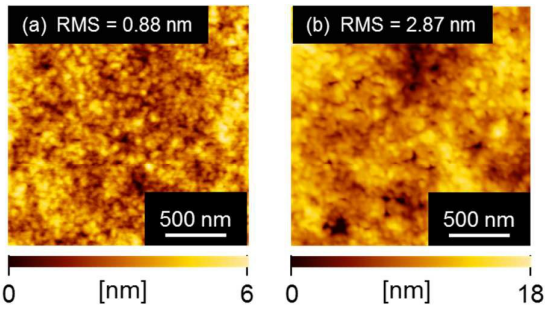

Figure 4 AFM images of polymer/PC$_{61}$BM blended films; (a) **P1** and (b) **P2**.

Grazing Incidence Wide-angle X-ray Scattering (GI-WAXS) Analysis of Polymer/PC$_{61}$BM Blended Films

To understand the detailed molecular orientation and packing structure of these two polymers, grazing-incidence wide-angle X-ray scattering (GI-WAXS) analysis was performed (Figure 5).[67] The **P1**/PC$_{61}$BM film fabricated on an ITO/ZnO substrate exhibited three orders of (*h*00) diffraction at 0.304 Å^{-1} on the q_z axis as spots, which corresponds to the lamellar structure of the polymers. In addition, ring-shaped (010) diffraction was observed from **P1** blended film at 1.73 Å^{-1} along both q_z and q_{xy} axes. These diffractions indicate that **P1** formed predominantly with an edge-on orientation, but the randomly oriented crystallite derived from the π-π stacking structure also coexisted. In contrast, the **P2**/PC$_{61}$BM film on the ITO/ZnO substrate showed intense (*h*00) diffraction up to fourth order at 0.310 Å^{-1} on the q_z axis, and obvious (010) diffraction at 1.78 Å^{-1} on the q_{xy} axis, although its diffraction peaks were slightly disordered. Furthermore, its interlayer distances in the lamellar (d_{lm} = 20.3 Å) and π-π stacking structures (d_{π} = 3.53 Å) as estimated from diffraction became shorter than those of **P1** (d_{lm} = 20.7 Å and d_{π} = 3.63 Å). This indicates that the introduction of fluorine atoms can enhance the crystallinity and suppress the disordering of molecular orientation. This may be due to strong intermolecular interactions induced by the strong dipole along the C-F bonds and the increased coplanarity of the polymer main chain. Among a number of synthesized PDT-based polymers, **P2** has the highest crystallinity in blended films on an ITO/ZnO substrate. This indicates that we can improve the crystallinity of PDT-based polymers by incorporating optimal acceptor units in the polymer backbone.

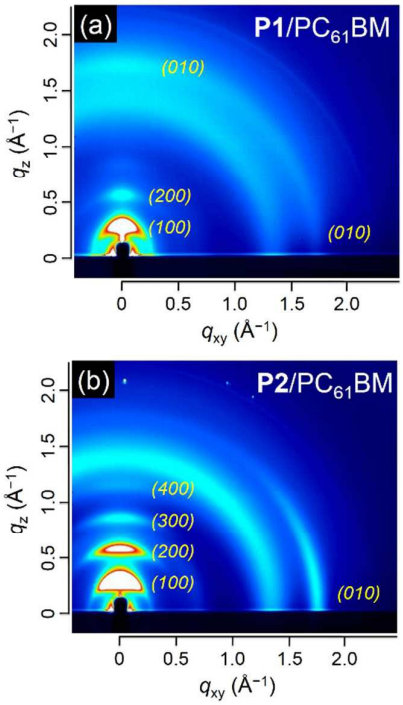

Figure 5 GI-WAXS image of polymer/PC$_{61}$BM films on ITO/ZnO substrate; (a) **P1** and (b) **P2**.

However, the predominantly edge-on orientation of both **P1** and **P2** is not suitable for solar cells.[68-70] In the case of **P1**, the solar cell showed a high FF of 0.67 owing to the existence of face-on crystallite along the π-π stacking direction in **P1** film, but its FF and J_{sc} decreased significantly in thick films. In contrast, the FF of **P2**-based cells was relatively low (0.59) even with thin films. Therefore, the highly oriented edge-on structure of these polymers, in particular **P2**, may prevent efficient carrier transport and reduce charge collection efficiency, resulting in low J_{sc}, and thus low PCE.

Characteristics of Field-Effect Transistor Devices

Since both PDT-based polymers adopted an unsuitable orientation for solar cells, we could not obtain high-performance PSCs. However, such a highly ordered edge-on orientation, with long-range order, is promising for high-

performance organic field-effect transistors (OFETs). To evaluate their potential as OFET materials, we fabricated and characterized typical bottom-gate top-contact OFETs with a 2 mm channel width (W) and a channel length (L) of 100 µm. *n*-Octadecyltriethoxysilane (ODTS) was used as a self-assembled monolayer (SAM). The highest device performances were obtained by thermal annealing at 250 °C for **P1** and 300 °C for **P2**. Figure 6 shows the best transfer and output curves, and the extracted device parameters are summarized in Table 4. Both OFET devices showed typical p-channel FET characteristics with the relatively low threshold voltage (V_{th}) of around −10 V. These devices also showed high on/off ratios up to 10^6 under ambient conditions, indicating high air-stability owing to their deep HOMO energy levels. Like the PSC, the **P2**-based OFET showed much higher performance than **P1**, with a hole mobility as high as 0.18 $cm^2\ V^{-1}\ s^{-1}$. AFM images of these polymer films on an ODTS-treated n^+-Si/SiO_2 substrate were quite different (Figure S4). Copolymer **P2** formed large crystalline grains and showed significant roughness (RMS 6.24 nm), while **P1** had a relatively smooth surface (RMS 0.81 nm). The continuous structure and large crystalline grains in **P2** film can provide an efficient channel and promote carrier transport. Therefore, **P2**-based OFETs exhibited higher hole mobility than **P1**-based.

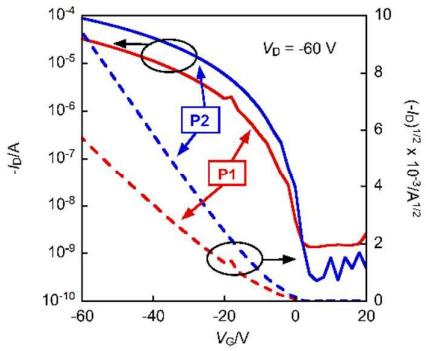

Figure 6 Transfer characteristics of **P1** (annealed at 250 °C) or **P2** (annealed at 300 °C)-based OFETs.

Table 4 OFET characteristics

polymer	μ_{FET} (μ_{avg})/$cm^2\ V^{-1}\ s^{-1}$ [a]	V_{th}/V[a]	$I_{on/off}$
P1	0.072 (0.053)	−10	10^4~10^5
P2	0.18 (0.10)	−10	10^4~10^6

[a]Estimated from transfer curves in saturation regime. [b]Average values based on more than 8 devices.

GI-WAXS Analysis of Polymer Films on n^+-Si/SiO_2 Substrate

GI-WAXS was used to refine our understanding of the molecular arrangements of **P1** and **P2** (Figure 7). In **P1** film on ODTS-treated n^+-Si/SiO_2 substrate, intense (h00) diffraction up to fourth order was observed on the q_z axis and (010) diffraction on the q_{xy} axis. Both diffractions appeared in opposite directions as very short arcs, indicating that face-on and edge-on arrangements coexisted in the **P1** film. The edge-on content was over 98%, roughly calculated from the intensities of the (100) diffraction in each direction, clearly showing a preferentially edge-on orientation. In contrast, the **P2** film also exhibited fourth-order lamellar diffraction on the q_z axis and obvious π-π stacking diffraction, but no peaks derived from face-on orientation were observed. In addition, the lamellar distance (d_{lm}) and π-π stacking distance (d_π) were 20.3 Å and 3.53 Å, shorter than in **P1**. The good ordering and dense packing structure of **P2** provide effective carrier transport, resulting in higher hole mobility than in **P1**. However, weak and arc-like peaks were observed in the (h00) diffraction, which suggests that **P2** film was contaminated with some slightly disordered crystallite. This may be due to the low molecular weight of **P2**, which typically affects the crystallinity and orientation mode of semiconducting polymers.[63] If we can improve the molecular weight of **P2**, we believe that developing a higher performance OFET device will be possible.

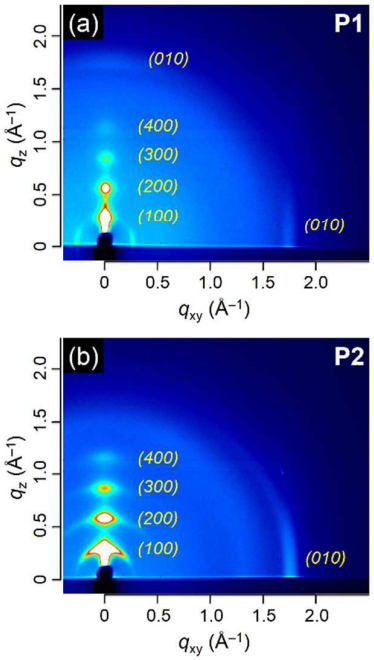

Figure 7 GI-WAXS image of polymer films on ODTS-treated n^+-Si/SiO_2 substrate; (a) **P1** annealed at 250 °C and (b) **P2** annealed at 300 °C.

Conclusions

We have synthesized new PDT-based semiconducting polymers that include benzothiadiazole (BT) derivatives. As in previous reports on PDT-based polymers, **P1** and **P2** have strong intermolecular interactions and sufficiently deep HOMO energy levels for high-performance PSCs. In particular, fluorine-substituted **P2** showed very strong aggregation behavior, but this feature limited its solubility, leading to a low molecular weight. When a BT unit with C_{2v} symmetry was incorporated in the polymer backbone, the present polymers formed a highly crystalline structure with a short π-stacking distance (3.53 Å) and well-ordered structure, even in films

blended with $PC_{61}BM$. We demonstrated that the introduction of an optimal acceptor moiety can increase the regularity of PDT-based polymers and enhance their π-orbital overlap with a neighboring polymer's main chain, leading to high crystallinity. However, the present polymer-based inverted PSCs showed a low PCE not exceeding 3.8% due to their low J_{sc} (~8 mA cm^{-2}), though they formed appropriate micro-phase separation structures. Their low solar cell performance is largely attributable to their molecular orientation in blended films. GI-WAXS analysis showed both polymers forming well-ordered crystallites in a predominantly edge-on manner, which is not a suitable orientation for high-performance PSCs, resulting in low J_{sc} and PCE.

On the other hand, a **P2**-based OFET device showed high hole mobility of up to 0.18 $cm^2\ V^{-1}\ s^{-1}$ owing to its optimal structure for OFETs. Its highly crystalline and dense packing structure can promote efficient carrier transport in OFET devices. However, a slightly disordered structure also coexisted in **P2** films on n^+-Si/SiO_2 substrates, caused by its low molecular weight, which may limit **P2**-based OFET performance. Therefore, further improvement in polymer structures is required for high-performance electronic devices. For example, the introduction of a longer branched alkyl chain at a different branching point may increase the solubility of the polymers without changing their molecular orientation or decreasing their crystallinity.[71] For PSCs, increasing the side chain attachment density on the polymer backbone is an effective strategy to create face-on orientation.[70] Thus, further modification of PDT-containing polymers is currently in progress.

Acknowledgements

This study was supported by ACT-C, JST and JSPS Grant-in-Aid for Young Scientists B (No. 26810129). GI-WAXS experiments were performed at BL19B2 and BL46XU of SPring-8 with the approval of the Japan Synchrotron Radiation Research Institute (JASRI) (Proposals 2014A1530 and 2014B1583). We gratefully thank Dr. Itaru Osaka (RIKEN, CEMS) and Dr. Tomoyuki Koganezawa (JASRI) for their evaluations of GI-WAXS images, Dr. Koichi Sakamaki and Mr. Mineki Hasegawa (ADEKA Corporation) for the DSC analysis, and GPC measurements, Prof. Koichi Mitsudo and Prof. Seiji Suga (Okayama University) for the CV measurements, Prof. Yoshihiro Kubozono and Ms. Shino Hamao (Okayama University) for the EQE measurements, Prof. Naoshi Ikeda (Okayama University) for the AFM images, and Ms. Megumi Kosaka and Mr. Motonari Kobayashi at the Department of Instrumental Analysis, Advanced Science Research Center, Okayama University, for the elemental analyses.

Notes and references

1 N. Espinosa, M. Hösel, M. Jørgensen and F. C. Krebs, *Energy Environ. Sci.* 2014, **7**, 855–866.
2 D. J. Lipomi and Z. Bao, *Energy Environ. Sci.,* 2011, **4**, 3314–3328.
3 S. Lizin, S. V. Passel, E. D. Schepper, W. Maes, L. Lutsen, J. Manca, and D. Vanderzande, *Energy Environ. Sci.,* 2013, **6**, 3136–3149.
4 T. R. Andersen, H. F. Dam, M. Hösel, M. Helgesen, J. E. Carle, T. T. Larsen-Olsen, S. A. Gevorgyan, J. W. Andreasen, J. Adams, N. Li, F. Machui, G. D. Spyropoulos, T. Ameri, N. Lemaître, M. Legros, A. Scheel, D. Gaiser, K. Kreul, S. Berny, O. R. Lozman, S. Nordman, M. Välimäki, M. Vilkman, R. R. Søndergaard, M. Jørgensen, C. J. Brabec and F. C. Krebs, *Energy Environ. Sci*., 2014, **7**, 2925–2933.
5 T. P. Osedach, T. L. Andrew, and V. Bulovic, *Energy Environ. Sci*., 2013, **6**, 711–718.
6 N. Espinosa, A. Laurent, F. C. Krebs, *Energy Environ. Sci*., 2015, **8**, 2537–2550.
7 Y. Liu, J. Zhao, Z. Li, C. Mu, W. Ma, H. Hu, K. Jiang, H. Lin, H. Ade, and H. Yan, *Nat. Commun.*, 2014, **5**, 5293/1–8.
8 J.-D. Chen, C. Cui, Y.-L. Li, L. Zhou, Q.-D. Ou, C. Li, Y. Li, and J.-X. Tang, *Adv. Mater.,* 2015, **27**, 1035–1041.
9 V. Vohra, K. Kawashima, T. Kakara, T. Koganezawa, I. Osaka, K. Takimiya, and H. Murata, *Nat. Photon.*, 2015, **9**, 403–409.
10 S. Zhang, L. Ye, W. Zhao, B. Yang, Q. Wang, and J. Hou, *Sci. China Chem*., 2015, **58**, 248–256.
11 M. Jeffries-EL, B. M. Kobilka, and B. J. Hale, *Macromolecules*, 2014, **47**, 7253–7271.
12 H. Zhou, L. Yang, and W. You, *Macromolecules*, 2012, **45**, 607–632.
13 Y. Li, *Acc. Chem. Res.*, 2012, **45**, 723–733.
14 Y. He, W. Hong, and Y. Li, *J. Mater. Chem. C*, 2014, **2**, 8651–8661.
15 L. Lu, T. Zheng, Q. Wu, A. M. Schneider, D. Zhao, and L. Yu, *Chem. Rev.*, 2015, DOI: 10.1021/acs.chemrev.5b00098.
16 X. Guo, N. Zhou, S. J. Lou, J. Smith, D. B. Tice, J. W. Hennek, R. P. Ortiz, J. T. L. Navarrete, S. Li, J. Strzalka, L. X. Chen, R. P. H. Chang, A. Facchetti and T. J. Marks, *Nat. Photon*., 2013, **7**, 825–833.
17 M. Saito, I. Osaka, Y. Suzuki, K. Takimiya, T. Okabe, S. Ikeda, and T. Asano, *Sci. Rep*., 2015, **5**, 14202/1–9.
18 W. Yue, R. S. Ashraf, C. B. Nielsen, E. Collado-Fregoso, M. R. Niazi, S. A. Yousaf, M. Kirkus, H.-Y. Chen, A. Amassian, J. R. Durrant, and I. McCulloch, *Adv. Mater*., 2015, **27**, 4702–4707.
19 J. W. Jo, J. W. Jung, E. H. Jung, H. Ahn, T. J. Shin, and W. H. Jo, *Energy Environ. Sci*., 2015, **8**, 2427–2434.
20 J.-H. Kim, J. B. Park, I. H. Jung, A. C. Grimsdale, S. C. Yoon, H. Yang, and D.-H. Hwang, *Energy Environ. Sci*., 2015, **8**, 2352–2356.
21 T. L. Nguyen, H. Choi, S.-J. Ko, M. A. Uddin, B. Walker, S. Yum, J.-E. Jeong, M. H. Yun, T. J. Shin, S. Hwang, J. Y. Kim, and H. Y. Woo, *Energy Environ. Sci*., 2014, **7**, 3040–3051.
22 A. J. Heeger, *Adv. Mater*., 2014, **26**, 10–28.
23 Y. Huang, E. J. Kramer, A. J. Heeger, and G. C. Bazan, *Chem. Rev*., 2014, **114**, 7006–7043.
24 Y. Nishihara, M. Kinoshita, K. Hyodo, Y. Okuda, R. Eguchi, H. Goto, S. Hamao, Y. Takabayashi and Y. Kubozono, *RSC Adv*., 2013, **3**, 19341–19347.
25 K. Hyodo, H. Nonobe, S. Nishinaga and Y. Nishihara, *Tetrahedron Lett.*, 2014, **55**, 4002–4005.
26 Y. Kubozono, K. Hyodo, H. Mori, S. Hamao, H. Goto, and Y. Nishihara, *J. Mater. Chem*. *C*, 2015, **3**, 2413–2421.
27 Y. Kubozono, X. He, S. Hamao, K. Teranishi, H. Goto, R. Eguchi, T. Kambe, S. Gohda and Y. Nishihara, *Eur. J. Inorg. Chem*., 2014, 3806–3819.
28 H. Mori, M. Suetsugu, S. Nishinaga, N.-H. Chang, H. Nonobe, Y. Okuda and Y. Nishihara, *J. Polym. Sci. Part A: Pol. Chem*., 2015, **53**, 709–718.
29 S. Nishinaga, H. Mori, and Nishihara, *Macromolecules*, 2015, **48**, 2875–2885.

30 S. Nishinaga, H. Mori, and Y. Nishihara, *Chem. Lett.*, 2015, **44**, 998–1000.
31 Z. Yi, S. Wang, and Y. Liu, *Adv. Mater.*, 2015, **27**, 3589–3606.
32 E. Wang, W. Mammo, and M. R. Andersson, *Adv. Mater.*, 2014, **26**, 1801–1826.
33 D. Mühlbacher, M. Scharber, M. Morana, Z. Zhu, D. Waller, R. Gaudiana, and C. Brabec, *Adv. Mater.*, 2006, **18**, 2884–2889.
34 J. You, L. Dou, K. Yoshimura, T. Kato, K. Ohya, T. Moriarty, K. Emery, C-C. Chen, J. Gao, G. Li, and Y. Yang, *Nat. Commun.*, 2013, **4**, 1446/1–10.
35 M. Zhang, H. N. Tsao, W. Pisula, A. K. Mishra, and K. Müllen, *J. Am. Chem. Soc.*, 2007, **129**, 3472–3473.
36 W. Zhang, J. Smith, S. E. Watkins, R. Gysel, M. McGehee, A. Salleo, J. Kirkpatrick, S. Ashraf, T. Anthopoulos, M. Heeney, and I. McCulloch, *J. Am. Chem. Soc.*, 2010, **132**, 11437–11439.
37 J. Peet, J. Y. Kim, N. E. Coates, W. L. Ma, D. Moses, A. J. Heeger and G. C. Bazan, *Nat. Mater.*, 2007, **6**, 497–500.
38 N. Blouin, A. Michaud, D. Gendron, S. Wakim, E. Blair, R. Neagu-Plesu, M. Belletête, G. Durocher, Y. Tao and M. Leclerc, *J. Am. Chem. Soc.*, 2008, **130**, 732–742.
39 S. H. Park, A. Roy, S. Beaupré, S. Cho, N. Coates, J. S. Moon, D. Moses, M. Leclerc, K. Lee and A. J. Heeger, *Nat. Photon.*, 2009, **3**, 297–303.
40 J. Hou, H.-Y. Chen, S. Zhang, G. Li and Y. Yang, *J. Am. Chem. Soc.*, 2008, **130**, 16144–16145.
41 R. C. Coffin, J. Peet, J. Rogers and G. C. Bazan, *Nat. Chem.*, 2009, **1**, 657–661.
42 Y.-J. Cheng, S.-H. Yang and C.-S. Hsu, *Chem. Rev.*, 2009, **109**, 5868–5923.
43 J. D. Yuen and F. Wudl, *Energy Environ. Sci.*, 2013, **6**, 392–406.
44 T. C. Parker, D. G. (Dan) Patel, K. Moudgil, S. Barlow, C. Risko, J.-L. Brédas, J. R. Reynolds and S. R. Marder, *Mater. Horiz.*, 2015, **2**, 22–36.
45 Q. Liu, X. Bao, S. Wen, Z. Du, L. Han, D. Zhu, Y. Chen, M. Sun and R. Yang, *Polym. Chem.*, 2014, **5**, 2076−2082.
46 D. Liu, C. Gu, M. Xiao, M. Qiu, M. Sun and R. Yang, *Polym. Chem.*, 2015, **6**, 3398−3406.
47 J. Ren, X. Bao, L. Han, J. Wang, M. Qiu, Q. Zhu, T. Hu, R. Sheng, M. Sun and R. Yang, *Polym. Chem.*, 2015, **6**, 4415−4423.
48 L. Ying, B. B. Y. Hsu, H. Zhan, G. C. Welch, P. Zalar, L. A. Perez, E. J. Kramer, T.-Q. Nguyen, A. J. Heeger, W.-Y. Wong, and G. C. Bazan, *J. Am. Chem. Soc.*, 2011, **133**, 18538–18541.
49 I. Osaka, M. Shimawaki, H. Mori, I. Doi, E. Miyazaki, T. Koganezawa, and K. Takimiya, *J. Am. Chem. Soc.*, 2012, **134**, 3498–3507.
50 Y. Wang, S. R. Parkin, J. Gierschner, and M. D. Watson, *Org. Lett.*, 2008, **10**, 3307–3310.
51 F. Babudri, G. M. Farinola, F. Naso, and R. Ragni, *Chem. Commun.*, 2007, 1003–1022.
52 K. Reichenbächer, H. I. Süss, and J. Hulliger, *Chem. Soc. Rev.*, 2005, **34**, 22–30.
53 H. Zhou, L. Yang, A. C. Stuart, S. C. Price, S. Liu, and W. You, *Angew. Chem. Int. Ed.*, 2011, **50**, 2995–2998.
54 B. A. DaSilveira Neto, A. S. Lopes, G. Ebeling, R. S. Gonçalves, V. E. U. Costa, F. H. Quina, and J. Dupont, *Tetrahedron*, 2005, **61**, 10975–10982.
55 I. Osaka, T. Abe, M. Shimawaki, T. Koganezawa, and K. Takimiya, *ACS Macro. Lett.*, 2012, **1**, 437–440.
56 J. Min, Z.-G. Zhang, and Y. Li, *Chem. Mater.*, 2012, **24**, 3247−3254.
57 Z. Chen, P. Cai, J. Chen, X. Liu, L. Zhang, L. Lan, J. Peng, Y. Ma, and Y. Cao, *Adv. Mater.*, 2014, **26**, 2586–2591.
58 Gaussian 09, Revision A. 02, M. J. Frisch, G. W. Trucks, H. B. Schlegel, G. E. Scuseria, M. A. Robb, J. R. Cheeseman, G. Scalmani, V. Barone, B. Mennucci, G. A. Petersson, H. Nakatsuji, M. Caricato, X. Li, H. P. Hratchian, A. F. Izmaylov, J. Bloino, G. Zheng, J. L. Sonnenberg, M. Hada, M. Ehara, K. Toyota, R. Fukuda, J. Hasegawa, M. Ishida, T. Nakajima, Y. Honda, O. Kitao, H. Nakai, T. Vreven, J. A., Jr. Montgomery, J. E. Peralta, F. Ogliaro, M. Bearpark, J. J. Heyd, E. Brothers, K. N. Kudin, V. N. Staroverov, R. Kobayashi, J. Normand, K. Raghavachari, A. Rendell, J. C. Burant, S. S. Iyengar, J. Tomasi, M. Cossi, N. Rega, N. J. Millam, M. Klene, J. E. Knox, J. B. Cross, V. Bakken, C. Adamo, J. Jaramillo, R. Gomperts, R. E. Stratmann, O. Yazyev, A. J. Austin, R. Cammi, C. Pomelli, J. W. Ochterski, R. L. Martin, K. Morokuma, V. G. Zakrzewski, G. A. Voth, P. Salvador, J. J. Dannenberg, S. Dapprich, A. D. Daniels, Ö. Farkas, J. B. Foresman, J. V. Ortiz, J. Cioslowski and D. J. Fox, Gaussian, Inc., Wallingford CT, 2009.
59 Y. Sun, J. H. Seo, C. J. Takacs, J. Seifter, and A. J. Heeger, *Adv. Mater.*, 2011, **23**, 1679–1683.
60 S. C. Price, A. C. Stuart, L. Yang, H. Zhou, and W. You, *J. Am. Chem. Soc.*, 2011, **133**, 4625–4631.
61 M. C. Scharber, D. Mühlbacher, M. Koppe, P. Denk, C. Waldauf, A. J. Heeger, and C. J. Brabec, *Adv. Mater.*, 2006, **18**, 789–794.
62 H. Zhou, L. Yang, S. Stoneking, and W. You, *ACS Appl. Mater. Interfaces*, 2010, **2**, 1377–1383.
63 I. Osaka, M. Saito, H. Mori, T. Koganezawa, and K. Takimiya, Adv. Mater., 2012, **24**, 425–430.
64 J. Subbiah, B. Purushothaman, M. Chen, T. Qin, M. Gao, D. Vak, F. H. Scholes, X. Chen, S. E. Watkins, G. J. Wilson, A. B. Holmes, W. W. H. Wong, and D. J. Jones, *Adv. Mater.*, 2015, **27**, 702–705.
65 W. Li, L. Yang, J. R. Tumbleston, L. Yan, H. Ade, and W. You, *Adv. Mater.*, 2014, **26**, 4456–4462.
66 G. Yu, J. Gao, J. C. Hummelen, F. Wudl, and A. J. Heeger, *Science*, 1995, **270**, 1789–1791.
67 J. Rivnay, S. C. B. Mannsfeld, C. E. Miller, A. Salleo, and M. F. Toney, *Chem. Rev.*, 2012, **112**, 5488–5519.
68 L. Yang, J. R. Tumbleston, H. Zhou, H. Ade, and W. You, *Energy Environ. Sci.*, 2013, **6**, 316–326.
69 I. Osaka, T. Kakara, N. Takemura, T. Koganezawa, and K. Takimiya, *J. Am. Chem. Soc.*, 2013, **135**, 8834–8837.
70 I. Osaka, and K. Takimiya, *Polymer*, 2015, **59**, A1–A15.
71 I. Kang, H.-J. Yun, D. S. Chung, S.-K. Kwon, and Y.-H. Kim, *J. Am. Chem. Soc.*, 2013, **135**, 14896–14899.

Highly Crystalline, Low Band-gap Semiconducting Polymers Based on Phenanthrodithiophene-benzothiadiazole for Solar Cells and Transistors

Hiroki Mori, Hikaru Nonobe and Yasushi Nishihara*

Newly developed PDT-benzothiadiazole copolymers formed high-crystalline film in a highly ordered edge-on manner. As the result, a fabricated solar cells and transistor devices showed a moderate PCE of ~3.8% and high hole mobility of up to 0.18 $cm^2 V^{-1} s^{-1}$.